Complex structure of the activating immunoreceptor NKG2D and its MHC class I-like ligand MICA

Pingwei Li¹, Daniel L. Morris¹, Benjamin E. Willcox², Alexander Steinle^{3,*}, Thomas Spies³ and Roland K. Strong¹

The major histocompatibility complex (MHC) class I homolog, MICA, is a stress-inducible ligand for NKG2D, a C-type lectin–like activating immunoreceptor. The crystal structure of this ligand-receptor complex that we report here reveals an NKG2D homodimer bound to a MICA monomer in an interaction that is analogous to that seen in T cell receptor–MHC class I protein complexes. Similar surfaces on each NKG2D monomer interact with different surfaces on either the $\alpha 1$ or $\alpha 2$ domains of MICA. The binding interactions are large in area and highly complementary. The central section of the $\alpha 2$ -domain helix, disordered in the structure of MICA alone, is ordered in the complex and forms part of the NKG2D interface. The extensive flexibility of the interdomain linker of MICA is shown by its altered conformation when crystallized alone or in complex with NKG2D.

T cells detect pathogens through specific interactions between T cell receptors (TCRs) on their surfaces and complexes of antigenic peptide fragments and polymorphic major histocompatibility complex (MHC) class I molecules on the surfaces of infected cells1. T cell activation requires an interaction between TCRs and appropriate MHC-peptide complexes in the context of appropriate costimulatory signals from engagement, for example, of the CD28 receptor on T cells with CD80 or CD86 ligands². Diverse cell surface molecules also modulate T cell activation, including the inhibitory and stimulatory receptors first identified on natural killer (NK) cells that are now recognized as being expressed on a range of cell types, including T cells. NK cells regulate innate and acquired immune responses through the release of various immune modulators (such as interferon-y) or by directly destroying virally infected or neoplastic cells. NK cell effector functions are regulated by integrating signals across the array of stimulatory and inhibitory NK cell surface receptors (NCRs) that are engaged upon interaction with target-cell surface NCR ligands³. Virally infected cells and tumor cells evade T cell-mediated immune surveillance by down-regulating the cell surface expression of MHC class I proteins4. Loss of NK cell inhibitory signals from NCRs that are specific for classical (HLA-A, HLA-B and HLA-C) or nonclassical (HLA-E) MHC class I proteins in this situation favors NK cell activation by altering the balance between stimulatory and inhibitory signals^{4,5}. Thus, NK cells can supplement T cell immune responses by detecting and eliminating such cells.

NCRs belong to two structural families. These are killer cell immunoglobulin-like receptors (KIRs), type I transmembrane glycoproteins containing one to three tandem immunoglobulin domains in the extracellular moiety, and homo- and heterodimeric type II transmembrane glycoproteins containing C-type lectin-like NK receptor domains (NKDs)⁶. NKDs lack the recognizable calcium-binding sites

that are conserved in true C-type lectins⁷. The NKG2 family of NKDs includes both activating and inhibitory NCRs: an example of this is the recognition of HLA-E in complex with a fragment of a leader peptide of a classical MHC class I protein by NKG2A-CD94 heterodimeric inhibitory receptors⁸. Crystal structures are available for members of both families. The KIR2DL1⁹, KIR2DL2¹⁰, KIR2DL3¹¹ proteins and KIR2DL2 complexed with human MHC class I protein HLA-Cw3¹² structure are solved, as are human NKD-CD94¹³ and murine NKD-Ly49A complexed with murine class I protein H-2D^{d14}.

NKG2D is an activating immunoreceptor that is expressed on most NK cells, CD8αβ T cells and γδ T cells. This makes it one of the most widely distributed NCRs currently known^{15,16}. Despite inclusion in the NKG2 family, NKG2D displays only limited sequence similarity to other members of the NKG2 family of NCRs and CD94 (20-30% identical) and forms homodimers, rather than heterodimers, with CD94, as do other NKG2 NCRs17. NKG2D engagement can be signaled by recruitment of phosphatidylinositol-3 kinase through the adapter molecule DAP1017,18. NKG2D ligands include the human cell-surface proteins MICA and MICB. These are distant MHC class I homologs that do not function in conventional antigen presentation or form heterodimers with β_2 -microglobulin (β_2 M), as do most other MHC class I proteins and homologs¹⁹⁻²¹. NKG2D-MIC recognition events stimulate effector responses from NK cells and γδ T cells and may positively modulate CD8αβ T cell responses^{16,22}. Unlike typical NCR ligands, which are constitutively expressed, MICA and MICB are induced by cellular stress^{21,22} and their tissue distribution is restricted to intestinal epithelium and epithelium-derived tumors^{21,23}. The uniform cytolytic response of diverse human $\gamma\delta$ T cell clones (of the $V_\delta 1$ family) or NK cell lines against target cells expressing various divergent human or nonhuman primate MIC proteins suggests a promiscuous interaction

¹Division of Basic Sciences, Fred Hutchinson Cancer Research Center, Seattle, WA 98109 USA. ²Division of Biology, California Institute of Technology, Pasadena, CA 91125, USA. ³Division of Clinical Research, Fred Hutchinson Cancer Research Center, Seattle, WA 98109, USA. *Present address: Interfakultäres Institut für Zellbiologie, Abteilung Immunologie, Auf der Morgenstelle 15, D-72076 Tübingen, Germany. Correspondence should be addressed to R. K. S. (rstrong@fhcrc.org).

ARTICLES

Table 1. Data collection and refinement statistics

Data collection and phasing							
Data set	Native	SeMet λ ₁	SeMet λ ₂	SeMet λ ₃			
Wavelength	1.100 Å	0.9567 Å	0.9793 Å	0.9794 Å			
Resolution	2.70 Å	3.25 Å	3.00 Å	3.20 Å			
High resolution shell	2.80-2.70 Å	3.37-3.25 Å	3.11-3.00 Å	3.31-3.20 Å			
Unique reflections	21,938	11,866	15,094	12,396			
Redundancy	11.7	10.0	10.2	9.85			
Completeness	99.9 (100.0)%	92.0 (93.2)%	92.8 (95.1)%	92.0 (92.5)%			
$< I/\sigma(I) >$	34.1 (4.1)	22.6 (6.7)	22.7 (4.2)	22.1 (6.0)			
R_{sym}	7.60 (42.5)%	11.1 (33.4)%	9.30 (41.4)%	10.3 (32.8)%			
Anomalous difference		6.69%	7.29%	7.64%			
Phasing power (centrics/acentrics)		0.93/0.82	1.28/1.23	1.52/1.35			

Overall figure-of-merit (20-3.25Å): 53.9%

	Refinement
Resolution	30-2.70 Å
Reflections (all F>0; working/test)	19,555/1,553
Protein/solvent atoms	4,263/47
R_{Cryst}/R_{Free}	22.7/28.2%
Average group B-factor	59.8 Ų
Wilson intercept	68.4 Ų
	Geometry
Bond length	0.007 Å
Bond angles	1.4°
	Ramachandran statistics ^b

Most favored	83.4%
Additional allowed	14.7%
Generously allowed	1.9%
Disallowed	0%

Values for the highest resolution shell are shown in parentheses. $R_{\text{sym}} \equiv \Sigma |I-<I>|I> \text{L}\rangle$ where I is the observed intensity, cI> is the mean intensity of multiple observations of symmetry-related reflections. Phasing power $\leq |F_H| > |E$ where F_H is the heavy atom structure factor amplitude and E is the residual lack-of-closure error. R_{Crystr} , $R_{\text{Free}} \equiv \Sigma ||F_{\text{obs}}| - |F_{\text{clic}}|/\Sigma ||F_{\text{obs}}|$ where F_{obs} and F_{calc} are the observed and calculated structure factor amplitudes. R_{Free} is calculated from a randomly chosen 7.5% of the reflections excluded from refinement⁵², $^{8}R.m.s.d.$ from ideality. ^{8}A nalyzed by PROCHECK⁵³.

between MIC proteins and NKG2D^{22,24}. Mapping the sequence conservations between these MIC proteins onto the crystal structure of human MICA²⁵ highlighted potential NKG2D binding sites on the underside of the α 1 α 2-platform domain, a surface normally rendered inaccessible by association with β_2 M in most MHC class I proteins and homologs.

We show here that, rather than the proposed interaction, an NKG2D homodimer is bound to the top of the MICA platform domain in an interaction that is analogous to $\alpha\beta$ TCR recognition of MHC class I proteins. The main feature of this complex is that the symmetrical surfaces on both halves of the NKG2D homodimer make near-equal contributions to the interaction by binding to distinctly different surfaces on the strictly asymmetric MICA platform.

Results

To determine the details of this key immunomodulatory recognition event, we determined the crystal structure of the complex formed between soluble bacterially expressed forms of the ectodomains of human MICA (allele 001) and human NKG2D using multiwavelength-anomalous dispersion (MAD) phases at a resolution of 2.7 Å (**Table 1**). Consistent with solution experiments (data not shown), NKG2D formed a homodimer that interacted with a single MICA monomer (**Fig. 1a,b**). The electron-density map was clear and continuous throughout, except

for residues 47–56 in MICA and also residues 80–88 of molecule A (NKG2D-A) and residues 80–92 of molecule B (NKG2D-B) in the NKG2D homodimer.

NKG2D structure

The overall fold of NKG2D was similar to other NKDs, with a root-mean-square deviation (r.m.s.d.) of <1.3 Å, despite limited sequence similarity (32-12% identical, Fig. 2). Whereas the hallmark secondary structure elements of canonical C-type lectins included two β sheets and two α helices which are conserved in the murine NKD Ly49A and the archetype of the C-type lectin fold family, mannose-binding protein (MBP)26—the fold of NKG2D was more similar to that of CD94, which retained only one of the α helices (corresponding to α 1 in NKG2D, Fig. 2). The most obvious difference between the structures of NKG2D and true C-type lectins involved the NH₂-terminal disulfide bond-containing subdomain (which consists of the NH2-terminal arms and loops and β strands 1 and 2 in NKG2D), which was very similar to a comparable structure in CD94 but absent in the crystal structure of MBP. The two canonical β sheets in C-type lectins and NKDs are conserved in NKG2D (1: β 1, β 2 and β 7; 2: β 3', β 3, β 4, β 5', β 5 and β 6, **Fig. 2**), although the second was more curved than CD94 or other NKDs and almost formed a β barrel. In NKG2D, CD94 and Ly49A, the first β sheet spanned the homodimer interfaces (in the crystal structure. CD94 formed homodimers which, it is proposed, recapitulate aspects of immunologically relevant CD94-NKG2 het-

erodimers¹³). NKG2D had an extra β strand (β 5'), which is not present in C-type lectins or other NKDs, and additional β strand-like elements in one of the extended NH₂-terminal arms (residues 93–95) and at the bottom of the homodimer interface (residues 148–150). Even though the loops corresponding to residues 148–150 in CD94 and Ly49A also formed part of their respective homodimer interfaces, the interaction was less extensive than in NKG2D where these residues formed hydrogen bonds across the homodimer interface. β 5' added a strand to the third β sheet that, along with a "stirrup" loop formed by residues 183–188, had the effect of creating a more saddle-shaped homodimer when compared to the relatively flat CD94 or Ly49A homodimers (**Fig. 2**). The canonical α 2 helix is absent in CD94 and replaced by a short five-residue-long 3₁₀ helix in NKG2D (**Fig. 2b**).

The two NKG2D monomers were very similar in structure and superimpose with an r.m.s.d. of $0.66 \, \mathring{A}$ on all common $C_{\alpha}s$. The homodimer symmetry axis of NKG2D was a near-perfect dyad (177°) that was markedly different from that of Ly49A (161°) ; the homodimer dyad axis of CD94 is crystallographic. NKG2D contained four intrachain disulfide bonds and no free thiols (**Fig. 2**). Whereas the intrachain disulfide-bonding pattern in the NH₂-terminal subdomain is conserved between NKG2D and CD94, with the first intrachain disulfide-forming cysteine (Cys⁹⁶) bonding to the third (Cys¹⁰⁵) and the second one (Cys⁹⁹)



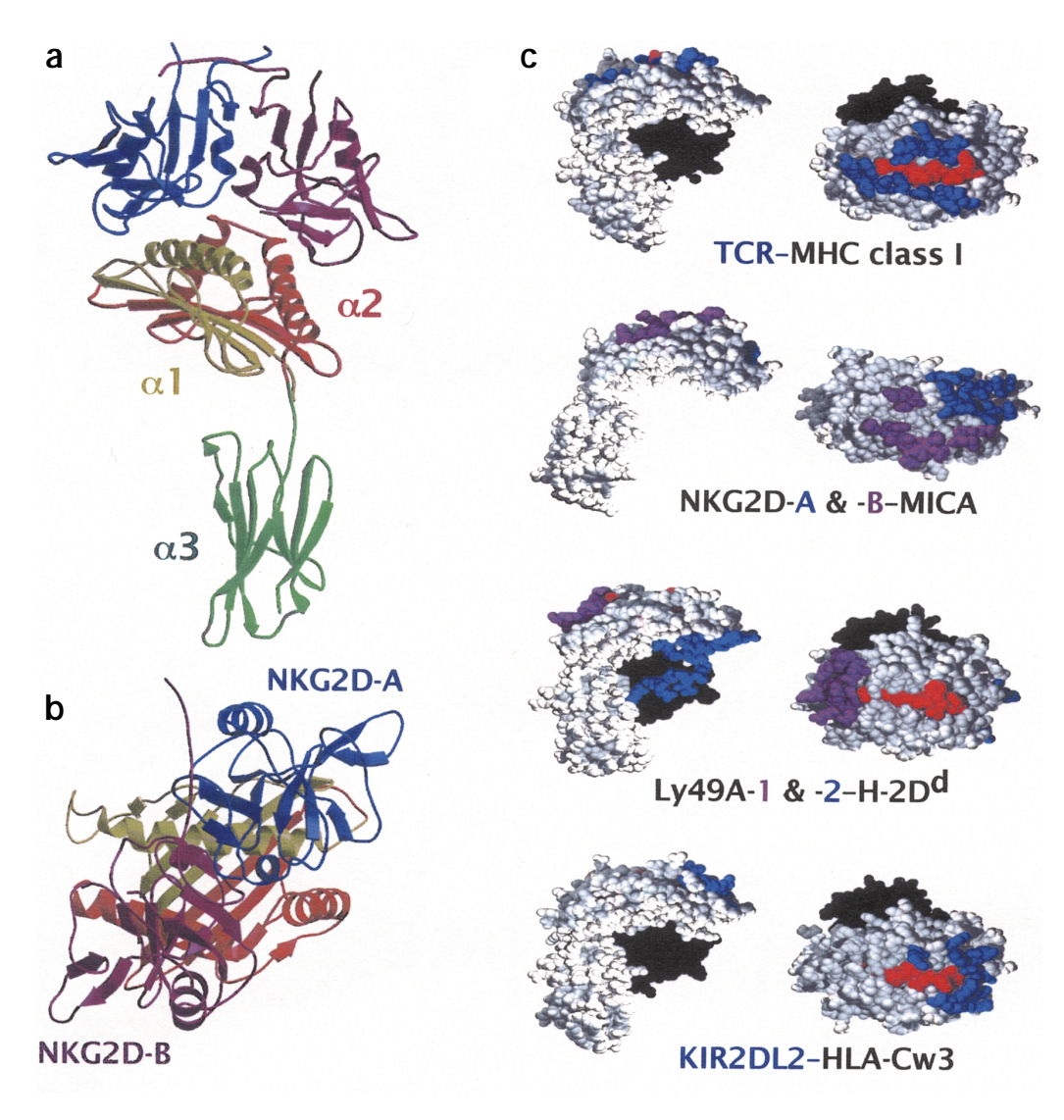


Figure 1. The structure of the NKG2D-MICA complex. (a) Side view and (b) top view (down the NKG2D homodimer dyad axis) of ribbon representations of the structure of the NKG2D-MICA complex. MICA domains are labeled and colored by domain (α 1, yellow; α 2, red; α3, green). NKG2D-A is blue and NKG2D-B is purple. (c) Footprints of TCR on HLA-A250, NKG2D (A and B) on MICA Ly49A on H-2Dd (both sites) and KIR2DL2 on HLA-Cw3 are blue or purple patches on space-filling representations of the structures of the MHC class I homolog (heavy chain, gray; β₂M, black; peptide, when present, red). Two orientations are shown for each molecule a side view on the left and a view from above on

echoes a rearrangement of the NH2-terminal arms, which cross over the homodimer interface and contact the neighboring molecule, as opposed to the case for CD94, where the NH2terminal arms run parallel along the homodimer interface. The NH2-terminal arm of NKG2D-B is more ordered than in any other related structure and is stabilized in the complex structure, in part, by crystal contacts. Because all the cysteine residues in the ectodomain of NKG2D are accounted for by intrachain disulfide linkages in the structure, NKG2D homodimers cannot be stabilized by interchain disulfide bonds. In CD94, the first cysteine in the

ectodomain (Cys⁵⁸) participates in a putative interchain disulfide bond with the corresponding cysteine conserved in other NKG2 family members. Other members of the NKG2 family of NCRs lack the cysteine corresponding to the third cysteine in NKG2D (Cys¹⁰⁵). This suggests that these molecules lack the corresponding intrachain disulfide bond seen in NKG2D, possibly in conjunction with altered conformations of the NH₂-terminal arms or subdomains.

Aside from the NH₂-terminal arms and subdomains, the largest differences in the backbones of NKG2D and CD94 occurred at the following locations: the loop NH₂-terminal to the 3_{10} helix (residues 140–143), with an outward movement of ~4 Å in NKG2D; the projecting tip of the $\beta 3_{10}^{-1}$ help, which moves ~6 Å downward toward the stirrup loop in NKG2D; and at the $\beta 5'$ - $\beta 5$ stirrup loop, which moves ~7 Å downward, closer to the homodimer interface (**Fig. 2**). The side chains of Phe¹⁰⁷ and Met¹⁰⁸ in CD94 also intercalated much more deeply into the CD94 homodimer interface than the corresponding residues in NKG2D (Leu¹⁴⁵ and Leu¹⁴⁶). The combination of this and the close approach of the β strand–like elements (residues 148–150) across the NKG2D interface resulted in the NKG2D homodimer closing down by ~13° relative to CD94, bringing the stirrup loops closer together (**Fig. 2**). The NKG2D

bonding to the fourth (Cys¹¹⁰), the spatial arrangement is different, the result of different spacings between cysteines in the sequences (Fig. 2). The NH₂-terminal two disulfide bonds in NKG2D are arranged in a ladder-like structure, one stacking nearly parallel to the next (with sulfurto-sulfur distances of 3.5-6.2Å) across the homodimer interface. Despite this proximity, the linkages are clearly intrachain, as determined both by electron-density maps and nonreducing SDS-polyacrylaminde gel electrophoresis (SDS-PAGE) analysis of recombinant protein (data not shown). In CD94, the corresponding disulfide bonds are more evenly distributed around the homodimer dvad axis (sulfur-to-sulfur distances of 7.5–12.7 Å). Differences in the spatial placement of the first disulfide bond (cysteines 96-105 in NKG2D or 59-70 in CD94) account for most of the alteration. In addition, the physical locations of the second disulfide bonds in NKG2D and CD94 (cysteines 99-110 in NKG2D or 61-72 in CD94) overlap well with each other and the first disulfide bond in Ly49A (cysteines 145-150) in structural superpositions (homologous sulfur-to-sulfur distances within 2.5 Å), even though the arrangement of corresponding cysteines in these three sequences is quite different (Fig. 2).

The altered arrangement of NH2-terminal disulfide bonds in NKG2D

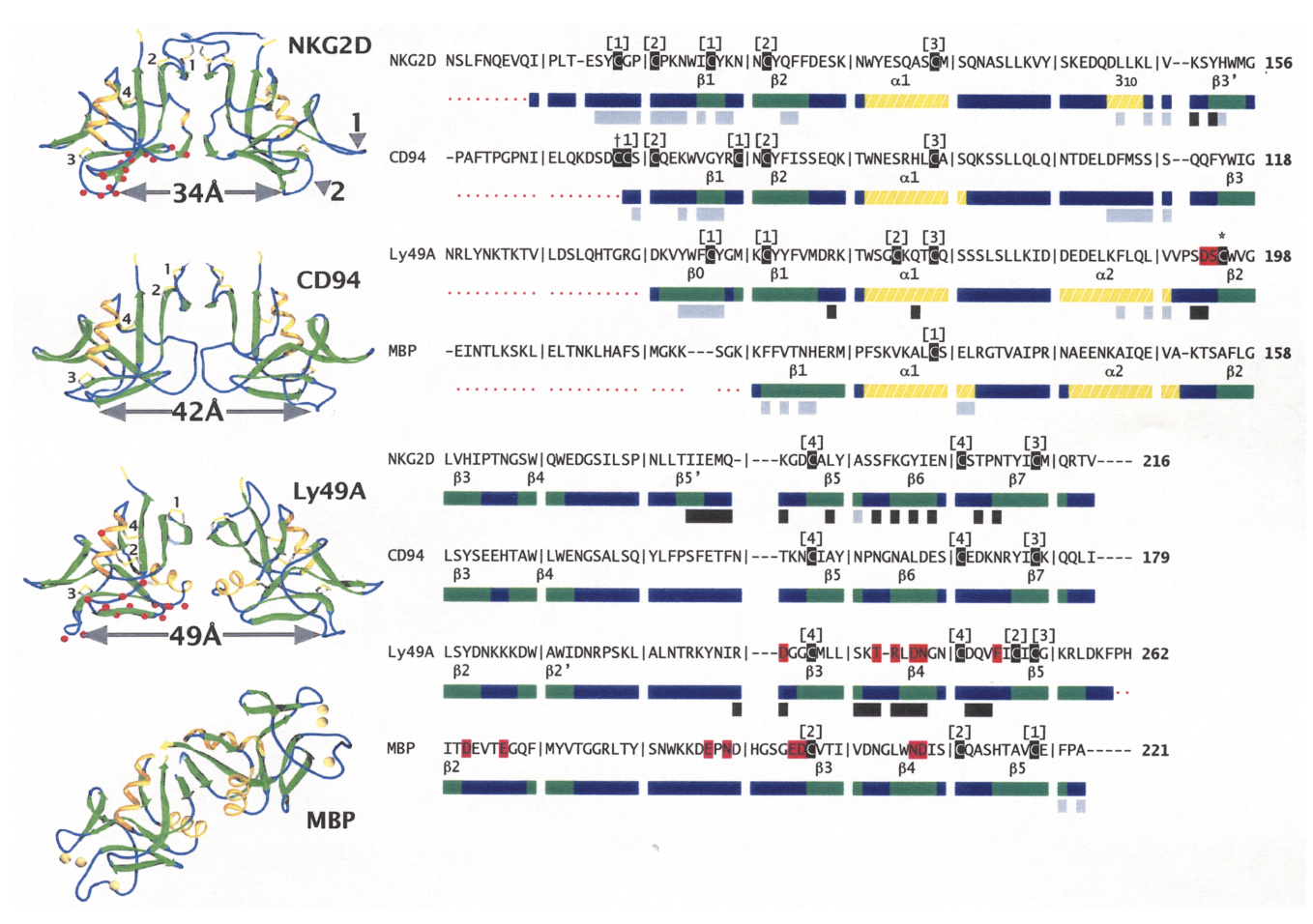


Figure 2. Comparisons of NKG2D with other NKDs and C-type lectins. Ribbon representations (left panels) of the homodimer structures of NKG2D, CD94 and Ly49A. For comparison purposes, the nonphysiological dimer observed in crystals of MBP, which was crystallized in the absence of its NH₂-terminal trimerization domain, is also shown. Secondary structure elements are delineated (α helices, yellow coils; β strands, green arrows; coil, blue tubes). Numbered arrows indicate features of the NKG2D structure discussed:1 is the β 3- β 4 loop; 2 is the β 5- β 5 stirrup loop. Residues comprising the ligand contact surfaces are mapped to one monomer of either NKG2D or Ly49A as red spheres, and calcium ions in the MBP structure are yellow spheres. The distances between corresponding features defining the binding surface saddles of NKG2D, CD94 and Ly49A are indicated. The views are oriented so that the left-hand monomers in each homodimer are in approximately equivalent orientations and with the homodimer dyad axis of NKG2D lying in the plane of the page. The alignment of the sequences of the ectodomains of human NKG2D, human CD94, murine Ly49A and rat MBP is structure-based (right panel). Dashes indicate gaps introduced to optimize the alignments. The residue numbering is indicated to the right of each sequence and a bar separates every ten-residue block. Cysteines are black, MBP cation ligands are purple and putative Ly49A carbohydrate ligands are red. Disulfide bond partners are indicated above each sequence, numbered, in brackets, by the order of the disulfide bonds in the particular sequence. The CD94 cysteine residue involved in a putative interchain disulfide bond is indicated by a dagger (†) and the free thiol in Ly49A is indicated by an asterisk (*). Secondary structure elements are indicated on the colored bars beneath each sequence (β strands, green; α helices, yellow; coil, blue; disordered, red dots) and have been numbered as in the original references; NKG2D secondary structure elements have been n

homodimer interface was composed of a series of main chain hydrogen bonds between homodimer-related $\beta 1$ strands and β strand-like elements (residues 148–150) in NKG2D-A and NKG2D-B sandwiched around a predominately hydrophobic core (**Table 2**). Additional cross-dimer hydrogen bonds involved residues in the NH₂-terminal arms and the body of the dimer-related protein. The NKG2D homodimer interface was highly complementary on the basis of the calculated shape correlation statistic (*Sc*), a measure of the degree that two contacting surfaces are a geometric match, with an *Sc* value of 0.69 (where an *Sc* value of 1.0 indicates a theoretically perfect fit)²⁷. The interface was also more extensive (2,170 Å² buried) than either the CD94 (1,200 Å²) or Ly49A (940 Å²) interfaces, but approached the size of the latter contact areas when residues from the NH₂-terminal arms (residues 89–95) were excluded (1390 Å²). A proposed carbohydrate-binding site on the surface

Ly49A¹⁴ was absent on NKG2D, the pocket being filled with the side chains of Glu²⁰¹ (glycine in Ly49A) and stirrup loop residues. As expected, NKG2D did not retain any of the features that are characteristic of the calcium-binding sites of C-type lectins (**Fig. 2**).

MICA structure

Like the heavy chain of other MHC class I proteins and homologs, the fold of MICA consisted of two structural domains: the $\alpha 1\alpha 2$ -platform domain and the C-type immunoglobulin-like $\alpha 3$ domain. In the crystal structure of MICA alone²⁵, the platform consisted of four distinct α helices arranged on an eight-stranded anti-parallel β sheet. These helices in MICA roughly corresponded to the two helices that define the peptide-binding groove in peptide-binding MHC class I proteins and homologs. The exception was the center section of the helical element

Table 2. In	termolecular	interactions v	within the	complex
NKG2D-A	MICA	Distance (Å)	Туре	MIC substitutions
	NKG2D resi	dues common	to sites A	and B
Tyr ¹⁵²	Lys ⁷¹		φ (3)	Gln
Tyr ¹⁵² OH	Arg ⁷⁴ NH	2.8	H bond	Lys
Tyr ¹⁵²	Met ⁷⁵	2.0	φ (2)	Arg, Lys
Ile ¹⁸²	His ⁷⁹		φ (1)	Tyr
Met ¹⁸⁴ O	Val ¹⁸ N	2.8	H bond	-
Met ¹⁸⁴	Val ¹⁸		φ (1)	_
Met ¹⁸⁴	Arg ⁷⁴		φ (1)	Lys
Met ¹⁸⁴	Ala ⁷⁸		φ (2)	Thr
Gln¹85 Oε	Val ¹⁸ O	3.0	H bond	_
Lys ¹⁹⁷ Νζ	Asp ¹⁴⁹ Oδ	3.8	Salt bridge	Asn, Glu
Tyr ¹⁹⁹	Met ⁷⁵		φ (3)	Arg, Lys
Tyr ¹⁹⁹ OH	His ⁷⁹ Nε	2.8	H bond	Tyr
Asn ²⁰⁷ Nδ	Arg ³⁸ NH	3.0	H bond	_
	•	residues uniq		Α
Glu ¹⁸³ O	Lys ⁸¹ Nζ	3.1	H bond	Gln
Lys ¹⁸⁶ Nζ	Asp ¹⁵ O	3.5	H bond	_
Lys ¹⁸⁶ N	Ser ¹⁷ Ογ	3.1	H bond	_
Glu ²⁰¹ Οε	Arg ⁷⁴ NH	3.4	Salt bridge	Lys
Thr ²⁰⁵ Oγ	Ser ²⁰ Oγ	3.5	H bond	_
NKG2D-B	MICA	Distance (Å)	Туре	MIC substitutions
	NKG2D resi	dues common	to sites A	and B
Tyr ¹⁵²	His156		φ (3)	Leu, Δ
Tyr ¹⁵²	Ala ¹⁵⁹		φ (2)	Thr, Δ
Ile ¹⁸²	Ala ¹⁶²		φ (1)	
Ile ¹⁸²	GIn ¹⁶⁶		φ (1)	Trp, Lys
Met ¹⁸⁴	His ¹⁵⁸		φ (2)	Arg, Δ
Met ¹⁸⁴	Ala ¹⁶²		φ (1)	_
Gln¹85Nε	His¹58 Nε	3.1	H bond	Arg, Δ
Lys ¹⁹⁷ Nζ	Asp ⁶⁵ Oδ	3.4	Salt bridge	_
Tyr ¹⁹⁹	Ala ¹⁵⁹		φ (4)	Thr, Δ
Tyr ¹⁹⁹ OH	Asp 163 O δ	2.4	H bond	Asn
Asn ²⁰⁷ Oγ	Thr¹55 Oγ	3.5	H bond	Ala
	NKG2E	residues uniq	jue to site	В
Lys¹50 Nζ	Ala ¹⁵⁰ O	3.3	H bond	Thr
Ile ¹⁸¹ O	Gln¹66 Nε	3.2	H bond	Trp, Lys
Leu ¹⁹¹	Thr ¹⁵⁵		φ (1)	Ala
Ser¹95 Oγ	Asp ¹⁶³ NH	3.2	H bond	Glu, Gly
NKG2D-A	NKG2D-B	Distance (Å)	Туре	
	Syn	nmetrical inte	ractions	
Ser ⁹⁴ N	Cys ⁹⁹ O	2.9	H bond	
Ser ⁹⁴ O	Cys ⁹⁹ N	2.8	H bond	
Tyr ⁹⁵ N	Cys ⁹⁶ O	3.5	H bond	
Lys ¹⁰¹ O	Glu ⁹³ N	3.4	H bond	
Cys ¹⁰⁵ N	Cys ¹⁰⁵ O	2.8	H bond	
lle ¹⁰⁴	Tyr ¹⁰⁶		φ (3)	
Phe ¹¹³	Leu ¹⁴⁸		φ (5)	
Lys ¹⁵⁰ N	Leu ¹⁴⁸ O	2.9	H bond	
Lys¹50 Nζ	Ser¹94 Oγ	3.1	H bond	
	Asyı	mmetrical inte	eractions	
Gly ⁹⁷ O	Ser ⁹⁴ O	3.0	H bond	
Ile ¹⁰⁴	Leu ¹⁴⁵		φ (1)	
Gln ²¹³ Oc	Glu ⁹³ Oc	3 /	H hond	

Hydrogen bonds (H bonds) are shown for donor-to-receptor distances of 2.4–3.5 Å with appropriate geometry, salt bridges for partners within 4.0 Å and hydrophobic interactions (ϕ) for carbon-to-carbon distances within 4.0 Å (the number of carbon/carbon pairs is in parentheses). Substitutions of MIC residues that contact NKG2D among the human MICA, MICB and nonhuman primate sequences known to bind to human NKG2D are shown as $\Delta^{22.24}$.

in the $\alpha 2$ domain (which corresponds to helix 2a in MHC class I proteins) where ten residues in MICA (residues 152–161) were disordered and presumed to form an extended flexible loop²⁵. The relative orientation of the two domains in the structure of free MICA was different from that of all other MHC class I proteins and related molecules resulting in an extended structure, with the platform of MICA flipped by over 110° from the position of the platform in other examples of class I folds.

The largest difference between the structure of MICA in complex with NKG2D and free MICA was the rearrangement of the platform and $\alpha 3$ domains in the two different crystals. When the $\alpha 3$ domains were superimposed, the angle between platform domains in the two forms was over 96°, which confirmed the proposed flexibility of the linker (Fig. 3a). We presumed that particular interdomain orientations seen in different MICA crystal structures in an otherwise extremely flexible molecule were selected by the extensive MICA-MICA crystal contacts that occur in these crystals. Despite the absence of an association with $\beta_2 M$, which bridges the platform and $\alpha 3$ domains in the MHC class I fold, the interdomain relationship in MICA in the MICA-NKG2D cocrystal structure was now within approximately 20° of all other MHC class I protein and homolog structures (Fig. 1c).

In a second major structural difference, the disordered loop in free MICA was now ordered, adding almost two turns of helix, which correspond to the canonical MHC class I α2 domain helix 2a and two residues of coil between helix 1 and 2a (Fig. 3b). Ordering of this loop was likely fostered by contacts with NKG2D (Table 2) and created a small pocket (roughly 6 Å wide × 6 Å deep × 14 Å long) that was similar in size and position to the ligand-binding pocket of serum Zn-α₂-glycoprotein (ZAG, Fig. 3c)²⁸. In the complex, the pocket was covered mostly by NKG2D-B, although a thin continuous channel ran through the complex between the MICAplatform helices and NKG2D. No residues from NKG2D penetrated the pocket. Unlike the ZAG pocket, which was hydrophobic in character, the MICA pocket was predominately lined with charged residues and limited at one end by a salt bridge between Asp72 and Lys¹⁵² (Fig. 3c). In comparison, the pocket was just large enough to accommodate the central segment (P3-P6) of the HLA-E peptide²⁹, but was occupied by only four well-ordered water molecules in the MICA-NKG2D cocrystal structure. There was no electron density that was unaccounted for by protein or water molecules that might have corresponded to a peptide- or nonpeptide-ligand bound in this pocket. It remained formally possible that this was the binding site for some small ligand that was not available in either baculoviral²⁵ or bacterial expression systems. However, steric clashes with NKG2D-B and the small size of the pocket would have severely limited the size of such a hypothetical ligand.

The r.m.s.d. for the superposition of the free and complexed forms of the MICA-platform domain was 1.00 Å (on 151 $C_{\alpha}s$), with the largest difference occurring at the loop containing helix 1 in the α 1 domain (residues 45–55, **Fig. 3d**). These residues were poorly ordered in the complex structure. Other, smaller, differences occurred in the conformation of the loops between helix 1 in the α 1 domain and strand 1 in the α 2 domain (residues 82–86) and between strand 4 and helix 1 in the α 2 domain (residues 131–134, **Fig. 3d**).

As noted in the structure of free MICA²⁵, a major difference between the structures of the platform domains of MICA and other MHC class I homologs occurred at two loops at the edge of the platform $\alpha 1$ domain (**Fig. 3e**). The loops between β strands 1 and 2 (residues 13–21 in MICA) and β strands 3 and 4 (residues 37–40

ARTICLES

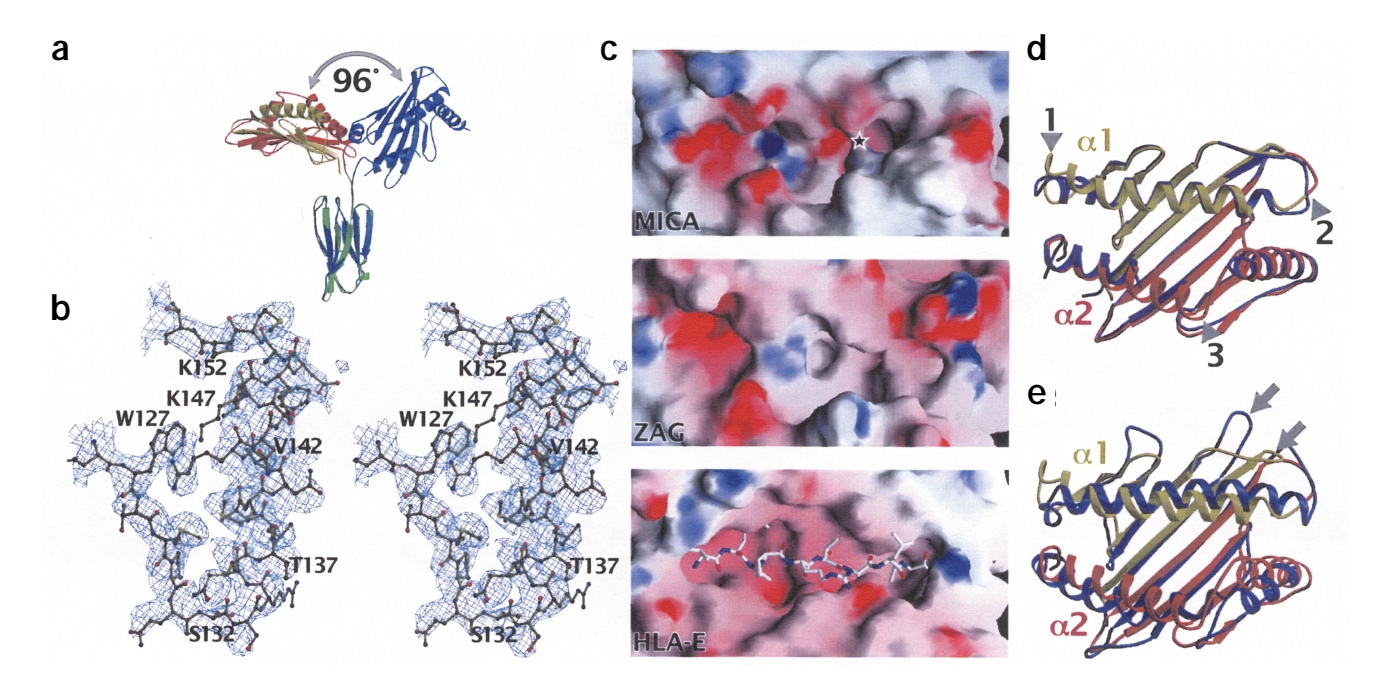


Figure 3.The structure of MICA in the complex. (a) Ribbon representations of the structure of MICA in complex with NKG2D, labeled and colored by domain (α1, yellow; α2, red; α3, green) and, in blue, crystallized on its own²⁵. The α3 domains have been used to superimpose the two molecules; the relative movement of α1α2-platform domains is shown. (b) A stereo view of the experimental MAD electron-density map, after density modification and phase extension, contoured at 1 σ , is shown in the region of the loop disordered in MICA when crystallized on its own. Residues from the final refined model are superimposed in ball-and-stick mode, labeled every five residues from Trp127 and colored by atom type (carbon, black; oxygen, red; nitrogen, blue; sulfur, yellow). (c) GRASP51 molecular surface representations of the pocket of MICA, the ligandbinding pocket of ZAG and the peptide-binding groove of HLA-E, colored by electrostatic potential. The bound peptide in the HLA-E structure is shown in stick representation colored by atom type. Residues with side chains lining the MICA pocket include, running roughly from left to right in this view: Glu¹67, Tyr7, Asp65, Leu66, Asp¹63, Arg⁰4, Asn69, Met¹⁶⁰, Glu⁹², Asp⁷² and Lys¹⁵². The star indicates the position of the salt bridge between residues Asp⁷² and Lys¹⁵². Superpositions of ribbon representations of the platform domains of (d) MICA in the NKG2D complex and alone (colored as in a) and (e) MICA in the NKG2D complex (colored as in a) and HLA-E (in blue)29 (d) The arrowheads indicate the loops (1 is between helix α 1 and helix α 2; 2 is between helix α 2 and the first β strand of the α 2 domain; 3 is the disordered loop) that are most different between the two crystal forms of MICA. MICA secondary structure elements are labeled as in²⁵. The B-factors for residues in the first two loops (1 and 2) are among the highest in the structure, possibly reflecting inherent conformational flexibility. We note that Asn⁵⁶ in the first of these loops (1) is a potential N-linked glycosylation site. Therefore, absence of an N-linked oligosaccharide in the bacterially expressed MICA used in this analysis may also contribute to the observed structural difference at this loop relative to baculovirus-expressed MICA²⁵. (e) The arrows indicate the different positions of the α1 domain β1-β2 loop in MICA and HLA-E.

in MICA) in the $\alpha 1$ domain projected equatorially from the platform domain of MHC class I proteins and homologs. In MICA, the \(\beta 1-\beta 2\) loop curled upward toward NKG2D, with differences of up to 9-10 Å between corresponding positions in the backbones; the β3-β4 loop was much shorter than in other MHC class I homologs (Fig. 3e). The MICA helices corresponding to the peptide groove-defining helices in MHC class I proteins and homologs were 2-9 Å closer together along their length than in peptide-binding MHC molecules (Fig. 3e). The largest relative movement of these helical elements occurred at the COOH terminus of helix 1 in the α 2 domain at the apex of a projection, or high point, on the surface of the platform. This high point (residues 148-155) included residues in the loop ordered in MICA in the NKG2D cocrystals but disordered in the structure of free MICA.

The MICA-NKG2D interface

The NKG2D homodimer diagonally overlaid the surface of the MICA platform in a manner that was analogous to the interaction of TCRs and MHC class I proteins: it made extensive contacts with the long helical elements conserved in all MHC class I homologs (Fig. 1a,b). Each NKG2D monomer predominately contacted either the $\alpha 1$ or $\alpha 2$ domains of MICA (Fig. 4a, b and Table 2). As in TCR-MHC class I interactions³⁰, the high point on the surface of the α 2 domain, between the α 1 and α 2a helices, prevented any other receptor orientation on this part of the platform domain overlying the region of the peptide-binding groove. NKG2D-B contacts on the $\alpha 2$ domain of MICA included residues in a loop that was disordered in the structure of MICA alone (Fig. 3a & 4b). Whereas KIR2DL2 contacted a roughly similar surface on HLA-Cw3, the two Ly49A contact surfaces on H-2Dd were quite dissimilar (Fig. 1c). However, whereas the D1 domain of KIR2DL2 occupied almost the same relative position on HLA-Cw3 as NKG2D-A does on MICA, the KIR2DL2 domain D2 bound to the other side of the α2 domain high point on HLA-Cw3 than NKG2D-B does on MICA (Fig. 1c).

The NKG2D-MICA interface consisted of a mixture of polar, hydrophobic and ionic interactions where the Ly49A-H-2Dd (site number 1) and KIR2DL2-HLA-Cw3 interfaces are dominated by ionic interactions (Table 2). The total buried surface area at the NKG2D-MICA interface (2180 Å²) was 20-25% larger than TCR-MHC class I interfaces, ~30% larger than the KIR2DL2-HLA-Cw3 interface, over twice the size of the Ly49A-H-2Dd interaction at site number1 and 30-40% larger than "average" protein-protein recognition interfaces31, but only about two-thirds of the area buried at the Ly49A-H-2Dd site number 2 interaction. The high overall shape complementarity²⁷ of the NKG2D and MICA surfaces at the binding sites (Sc=0.72) was much greater than antibody-antigen (Sc=0.64–0.68), TCR-ligand (Sc=0.46-0.63) or other NCR-ligand interactions (Sc=0.58 for KIR2DL2-HLA-Cw3), except for the Ly49A-H-2Dd site



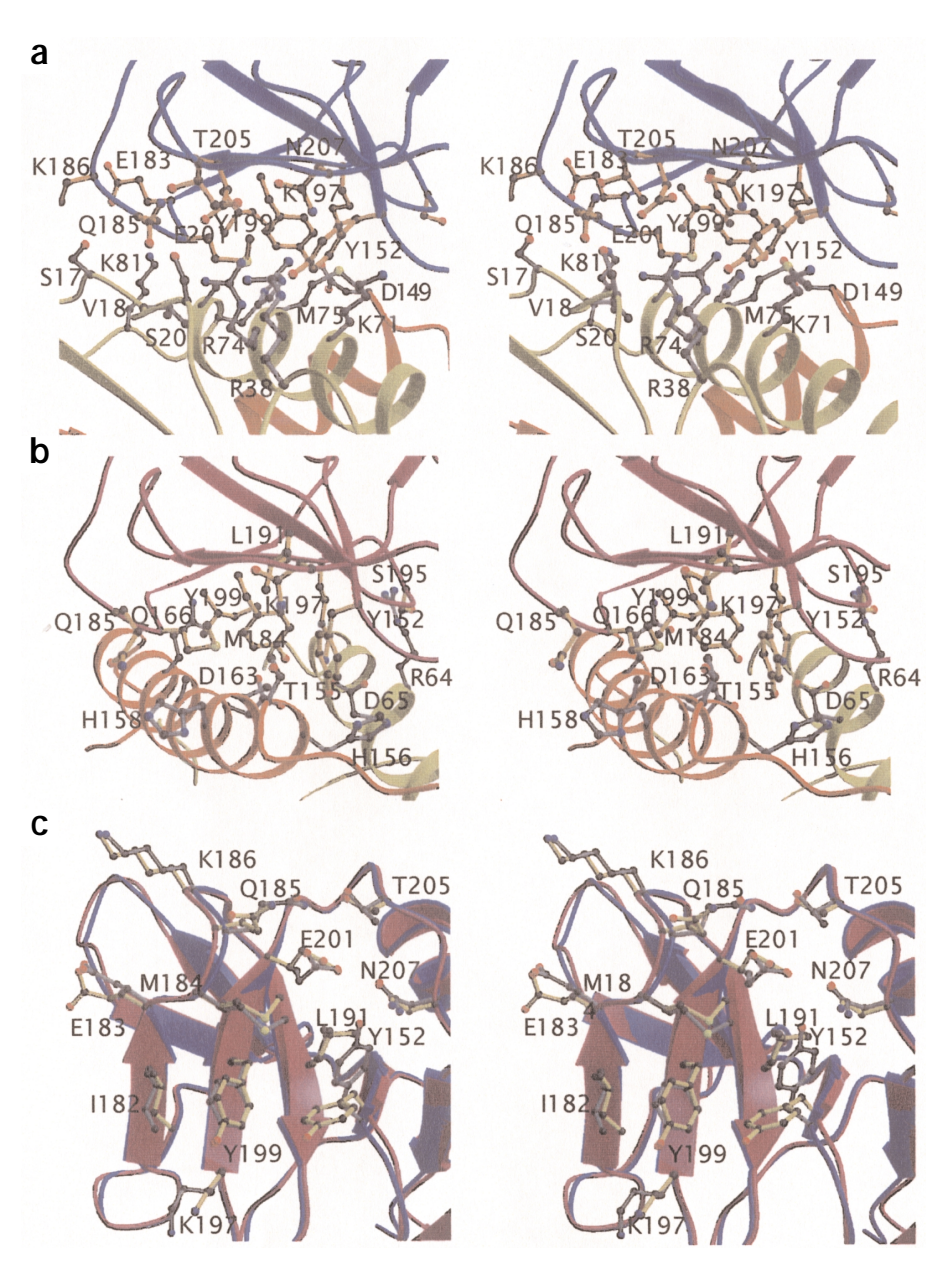


Figure 4. Details of the binding sites. Stereo views of (a) the NKG2D-A–MICA and (b) NKG2D-B–MICA interaction surfaces. Ribbon representations of the NKG2D and MICA backbones, colored by chain (as in Fig. 1), and side chains of key residues, colored by atom type, are shown. In these two views, NKG2D-A and NKG2D-B are shown in identical orientations. (c) A stereo view of the superposition of the MICA binding sites on the two NKG2D monomers, colored as above. The backbone of NKG2D is shown in ribbon representation and binding site residues are shown in ball-and-stick mode and labeled.

a dissociation rate constant at 37° of 0.04 s⁻¹ (corresponding to a $t_{1/2}$ of 17 s), which indicated that the NKG2D-MICA interaction may be relatively more stable than TCR-ligand and other NCR-ligand complexes. The association rate constant (k_{on}), 4×10^4 – 7×10^4 M-1s-1, was slow relative to many other cell surface interactions, which typically have k_{on} ≥1×10⁵ M⁻¹s⁻¹ (ref. 38). Also, measurements at 25 °C and 37 °C indicated that both association and dissociation rate constants are somewhat temperature dependent, which indicated activation energy barriers impede association and dissociation (Fig. 5). These features-both of which are shared by TCR-MHC interactions, where binding is thought to be accompanied by a reduction in flexibility at the receptor-ligand interface38were consistent with an extensive highly complementary NKG2D-MICA interaction where the flexible loop on MICA (residues 152-161) must become ordered during complex formation. The interdomain flexibility in MICA was less likely to contribute to this effect as neither conformation observed in the crystal structures nor many of the possible interdomain arrangements would impose steric hindrances to NKG2D binding.

number 1 interaction (Sc=0.78). Unlike the Ly49A–H-2D^d interface, none of the three NKG2D or eight MICA potential N-linked glycosylation sites lay near the interface. Thus, we deduced that binding is solely mediated by direct protein-protein contacts. Consistent with this deduction, NKG2D failed to retain any recognizable remnant of the saccharide-binding site of true C-type lectins or the proposed saccharide-binding site of Ly49A¹⁴ (**Fig. 2**).

Strength and stability of the MICA-NKG2D interaction

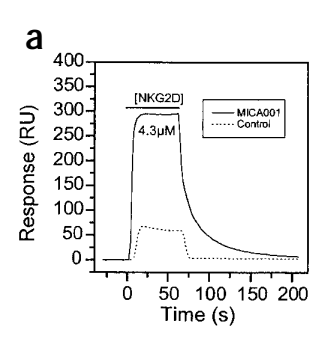
To quantify the affinity and kinetics of NKG2D binding to MICA, we analyzed the interaction by surface plasmon–resonance (SPR) methods. The resulting equilibrium dissociation constant (K_D), 1 μ M at 37°, was one to two orders of magnitude stronger than most NCR and many TCR interactions with host MHC proteins, where dissociation constants are typically in the tens-of-micromolar range^{12,32–37}. Kinetic analysis yielded

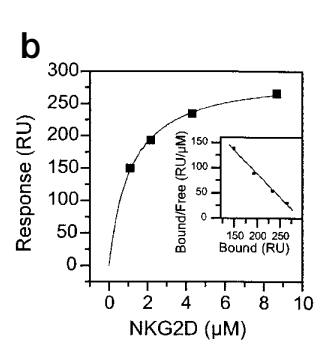
Higher-order complexes

Contacts in the crystal were dominated by extensive (3400 $\mbox{Å}^2$ buried) MICA-MICA contacts around the crystallographic four-fold

axis and an additional, minor (840 Ų buried) crystal contact between NKG2D and the $\alpha 3$ domain of a MICA molecule in a neighboring complex. However, the resultant MICA tetramer is unlikely to form on cell surfaces because five of the eight asparagines at potential N-linked glycosylation sites in MICA (residues 8, 102, 187, 212 and 239) were buried in the tetramer interface. In addition, the MICA COOH termini were too far away from where the bottom of the tetramer limited approach to the membrane. The NKG2D-MICA $\alpha 3$ domain contact is also unlikely to be physiologically relevant, due to the limited extent of this interaction and the topological incompatibility between the formation of this complex and the two membrane surfaces involved. Therefore, we saw no higher-order complexes in the crystal structure that are likely to be informative about possible signaling mechanisms at the cell surface. As in the structure of free MICA, no major contacts were found between domains within a single MICA molecule that might contribute to stabilizing this particular interdomain







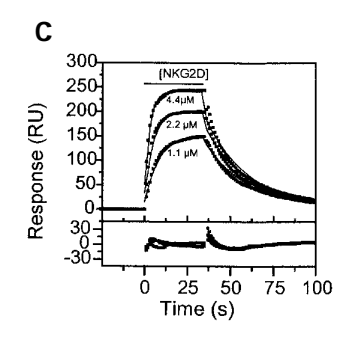


Figure 5. Affinity and kinetics measurements of the NKG2D–MICA interaction by SPR. (a) Equilibrium binding measurements of bacterially expressed NKG2D injected (solid bar) at 5 μ l/min over surfaces with either baculovirus-expressed MICA or control protein immobilized. The response is greater over the MICA surface (solid trace) than the control (dotted trace), which indicates specific binding. (b) A nonlinear curve fit of the 1:1 Langmuir binding isotherm to 37 °C MICA equilibrium binding data (solid squares). The predicted R_{max} =297 resonance units; K_0 =1 μ M. Inset: a Scatchard plot of the same data (K_0 =1 μ M). (c) Kinetic measurements are shown, made at 37 °C by injecting NKG2D (50 μ l/min) at a range of concentrations over MICA and control surfaces. The data plotted (filled squares) have had the background response subtracted. The results of globally fitting rate equations derived from the 1:1 Langmuir binding model are shown as solid lines and residual errors from the fits are shown in the bottom panel. The kinetic constants obtained (K_{on} -6.75×10⁴ M⁻¹s⁻¹, K_{off} =0.039 s⁻¹) predict an affinity of 0.6 μ M, similar to that obtained from equilibrium binding analysis. Analogous kinetic measurements at 25 °C yielded a K_{on} of 4.26×10⁴ M⁻¹s⁻¹ and a K_{off} of 0.013 s⁻¹ (calculated dissociation constant K_{Deale} was 0.3 μ M).

conformation.

Discussion

The NKG2D homodimer bound to MICA through a surface on the side of the homodimer opposite the NH2-termini, which was comparable to the ligand-binding surface of Ly49A14, the proposed ligand-binding surface of CD9413 and close to the carbohydrate-binding pocket of MBP26. The increased curvature of the binding surface saddle of NKG2D, due to the stirrup loops and interdomain relationship, precisely complemented the decreased interhelical distances of MICA relative to other MHC class I homologs. Thus, NKG2D was sterically incompatible with other MHC class I protein or homolog platform-domain structures and other NKDs would be a poor match for MICA. Essentially identical, homodimer dyad-related surfaces on NKG2D-A and NKG2D-B made comparably extensive and complementary contacts with different surfaces on either the $\alpha 1$ or $\alpha 2$ domains of MICA respectively. This contrasts with other situations, such as the interactions between other homodimeric receptors and monomeric ligands, where one subunit of the symmetric receptor dominated the interaction with the asymmetric ligand (both Ly49A binding sites on H-2D^{d14} and CD8αα binding to HLA-A239 or H-2Kb40), or the binding of multiple copies of receptors to a single asymmetric ligand. The latter is exemplified by the human growth hormone receptor-ligand complex41, where interdomain flexibility in the receptor allowed the adoption of different conformations to bind to multiple distinct surfaces on the hormone ligand.

Whereas an α helix constituted the central element of both binding sites on MICA, the side chains that were actually making contacts with NKG2D were essentially completely different (running from one end to the other of the α 1 helix: LysArgMetAlaHisLys *versus* ThrHisAlaAla ArgGln in the α 2 helix). Whereas the structure of the NKG2D-A contact surface was essentially unchanged in free and complexed forms of MICA, seven residues contacted by NKG2D-B were part of the disordered loop in free MICA. Both NKG2D monomers also made contacts to the other MICA domain: NKG2D-A contacting Asp¹⁴⁹ in α 2 and NKG2D-B contacting Asp⁶⁵ and Asp¹⁶³ in α 1. NKG2D-A also interacted with residues 15, 17, 18 and 20 in the β 1- β 2 loop in the α 1 domain, which accounted for its markedly altered conformation relative to other MHC class I

homologs. The NKG2D surfaces, however, were quite similar. Eleven residues in both NKG2D-A and NKG2D-B contacted MICA, of which seven were common to both contact surfaces. These seven residues defined a core binding site on NKG2D that dominated the intermolecular contacts with MICA at both interfaces. However, six of these seven residues made different contacts at either the NKG2D-A-MICA or the NKG2D-B-MICA interfaces; the seventh residue, Lys197, participating in a common salt bridge to an aspartic acid at both binding sites (Asp149 or Asp163 in MICA).

The recognition of an asymmetric ligand by a symmetric receptor was achieved by a core-binding surface on NKG2D that can specifically interact with two distinct surfaces

on MICA with few conformational changes or substitution of contacts. The largest conformational differences occurred at Tyr¹⁵² (where the hydroxyl oxygen moved almost 6.5 Å and the ring rotated by 90° in the ring plane and 65° perpendicular to the ring), at Lys¹⁹⁷ (where the N ζ moved over 4 Å) and at Gln¹⁸⁵ and Glu²⁰¹ (where the side chains used different rotamers). There was little induced conformational change in the backbone structure of the two NKG2D monomers; the r.m.s.d. for the superposition of MICA contacting elements (residues 150–152 and 180–207 in NKG2D) was only 0.36 Å on all backbone atoms.

NKG2-CD94 heterodimers bind, in a peptide-specific manner, to HLA-E 8 . A model for the NKG2-CD94 heterodimer was proposed on the basis of the structure of the CD94 homodimer. In addition, the interaction with HLA-E was proposed to be similar to that in a TCR-MHC complex, although the orientation of the heterodimer on the HLA-E platform could not be given in detail 12 . We noted that superimposing CD94 onto NKG2D, and the HLA-E platform onto MICA, generated, with only minor adjustments, a reasonable model NKG2-CD94-HLA-E complex. In this complex, CD94 sits on the α 1 domain of HLA-E (corresponding to NKG2D-A) and the NKG2 moiety sits on the α 2 domain, with a small hydrophobic patch on CD94 (Phe 114 and Leu 162) matching a similar patch on HLA-E (Ile 73 , Val 76 and the side chain of the P8 residue in the peptide, Leu in the crystal structure).

As demonstrated by the details of the MICA interaction, NKG2D has evolved a single binding site that is competent to specifically bind to two distinct protein surfaces. Reports that human NKG2D binds to various human MICA and MICB alleles and nonhuman primate MIC proteins^{22,24} also demonstrated a remarkable tolerance for sequence substitutions in the MIC binding sites. Though no recognizable rodent MIC homologs have been identified, the ectodomains of human and murine NKG2D are highly conserved (69% identical). Murine NKG2D ligands include the distant MHC class I homologs Rae1 and H-60⁴², which are also quite unlike MICA. How murine NKG2D interacts with these ligands, and how human NKG2D interacts with other potential human ligands, remains unclear. This divergence of specificity implies that NKG2D has evolved mechanisms to recognize a variety of protein surfaces, apparently without using flexible elements of structure beyond relatively small changes in a handful of side chain conformations.



Methods

Protein expression, crystallization and crystallography. The extracellular domains of human MICA (residues 1-276) and human NKG2D (residues 80-216) were expressed in bacteria and refolded as complexes from inclusion bodies. Proper folding was analyzed by solution monodispersivity of the purified concentrated protein, as determined by size-exclusion chromatography (SEC) and dynamic light scattering, and also the presence of a single disulfide-bonded species by nonreducing PAGE analysis. A selenomethionine (SeMet) derivative of MICA was prepared as described44 and refolded separately; NKG2D-SeMet-MICA complexes were then isolated by SEC. The MICA-NKG2D complex was crystallized by sitting-drop vapor diffusion at 22 °C from a solution containing 7.5 mg/ml of protein, 25 mM PIPES (pH 7.0), 1 mM EDTA and 0.02% NaN3 mixed at a ratio of 1:1 with a well solution containing 0.4 M (NH₄)₂SO₄ and 50 mM MES (pH 6.5). The space group of the crystals was P42₁2 (a=b=122.78Å, c=102.82Å) with one complete MICA monomer-NKG2D homodimer complex per asymmetric unit, which resulted in a V_m of 3.0Å³ per Dalton. Crystals were cryopreserved by stepwise transfer to mother liquor + 30% glycerol. Diffraction data from native and SeMet crystals were collected at ALS beamline 5.0.2 with the use of a Quantum-4 CCD detector and reduced with HKL45. All eight selenium sites in MICA were located by automated Patterson search and multiwavelength anomalous dispersion phases were calculated with the Crystallography & NMR System (CNS) package⁴⁶. After solvent flipping and phase extension in CNS, the electron-density map was clear and unambiguous. Models of MICA (Protein Data Bank number 1B3J) and CD94 (Protein Data Bank number 1B6E) were manually docked into this map and subsequently rebuilt with O⁴⁷.

The structure was refined in CNS (against all F>0) with overall anisotropic B-factor and bulk solvent corrections applied. Initial torsional simulated-annealing refinement, using the maximum likelihood target function mlhl, was followed by positional refinement using the mlf target function. The progress of the refinement was confirmed by the monotonic decrease in both $R_{\rm Cyst}$ and $R_{\rm Fine}$. NCS restraints were not imposed because of the breakdown of symmetry in the NKG2D homodimer at the MICA binding sites and the NH₂-termini. Coordinates have been deposited in the Protein Data Bank with accession code 1hyr⁴⁸.

SPR measurements. Experiments were done in HBS-EP buffer with a Biacore 2000 instrument (Biacore AB, Uppsala, Sweden). To conduct equilibrium-binding measurements at 37 °C, bacterially expressed NKG2D was injected over either baculovirus-expressed MICA49 or a control protein amine-coupled to a CM5 sensor chip. Injections of NKG2D were repeated over a range of concentrations and the amount of binding at each concentration (in Fig. 5b) was calculated as the difference in the response at equilibrium in the MICA and control flow cells. For Scatchard analysis, the K_D value (1 μ M) was obtained from the slope of the plot (K_D =-1/slope) by linear regression. For kinetic analysis, rate equations derived from the 1:1 Langmuir binding model were fitted simultaneously to association and dissociation phases of all three injections (global fitting) with the use of BIAevaluation $3.0\ software$. Data collection at progressively higher flow rates (to 100 µl/min) and over flow cells with progressively lower MICA expression immobilized excluded mass transport limitations. The slow off-rates obtained (k_{off} =0.013 s⁻¹ at 25 °C) explain the ability to isolate complexes by size-exclusion chromatography, despite the relatively low affinity. Binding responses over bacterially expressed MICA coupled to chips were similar to those over baculovirally expressed MICA, which suggested that glycosylation in insect cells does not affect the interaction. The activity of NKG2D was judged to be near 100% on the basis of size-exclusion chromatography in the presence of MICA (data not shown). Protein was quantified by bicinchoninic (BCA) assay (Pierce, Rockford, IL).

Note added in proof: The structure of human NKG2D in the complex recapitulated all the salient features of the recently reported structure of murine NKG2D⁴³.

Acknowledgements

We thank L. Hung, G. McDermott and T. Earnest (Advanced Light Source, Lawrence Berkeley National Laboratory) for assistance with data collection. Supported by National Institutes of Health grants AI42200 (to R. K. S.), CA18221 and AI30581 (to T. S.).

Received 20 February 2001; accepted 23 March 2001

- Germain, R. N. & Margulies, D. H. The biochemistry and cell biology of antigen processing and presentation. Ann. Rev. Immunol. 11, 403–450 (1993).
- Lenschow, D. J., Walunas, T. L. & Bluestone, J.A. CD28/B7 system of T cell costimulation. Annu. Rev. Immunol. 14, 233–258 (1996).
- 3. Lanier, L. L. Turning on natural killer cells. J. Exp. Med. 191, 1259–1262 (2000).
- 4. Ravetch, J.V. & Lanier, L. L. Immune inhibitory receptors. Science 290, 84–89 (2000)
- Lee, N. et al. HLA-E is a major ligand for the natural killer inhibitory receptor CD94/NKG2A. Proc. Natl Acad. Sci. USA 95, 5199–5204 (1998).
- Weis, W. I., Taylor, M. E. & Drickamer, K. The C-type lectin superfamily in the immune system. Immunol. Rev. 163, 19–34 (1998).
 Drickamer, K. Ca²-dependent carbochydrate-recognition domains in animal proteins. Curr. Opin.
- Struct. Biol. 3, 393–400 (1993).

 8. Lopez-Botet, M. & Bellon, T. Natural killer cell activation and inhibition by receptors for MHC class I.
- Lopez-Botet, M. & Bellon, I. Natural killer cell activation and inhibition by receptors for MHC class
 Curr. Opin. Immunol. 11, 301–307 (1999).
 Top. O. D. et al. Structure of the inhibitions recented for human patural killer cells recembles.
- Fan, Q. R. et al. Structure of the inhibitory receptor for human natural killer cells resembles haematopoietic receptors. Nature 389, 96–100 (1997).
 Snyder, G.A., Brooks, A. G. & Sun, P. D. Crystal structure of the HLA-Cw3 allotype-specific killer cell
- inhibitory receptor KIR2DL2. *Proc. Natl Acad. Sci. USA* **96**, 3864–3869 (1999).

 11. Maenaka, K., Juji, T., Stuart, D. I. & Jones, E.Y. Crystal structure of the human p58 killer cell inhibitory
- Maenaka, K., Juji, T., Stuart, D. I. & Jones, E.Y. Crystal structure of the human p58 killer cell inhibitory receptor (KIR2DL3) specific for HLA-Cw3-related MHC class I. Structure 7, 391–398 (1999).

- Boyington, J. C., Motyka, S. A., Schuck, P., Brooks, A. G. & Sun, P. D. Crystal structure of an NK cell immunoglobulin-like receptor in complex with its class I MHC ligand. Nature 405, 537–543 (2000).
- Boyington, J. C. et al. Structure of CD94 reveals a novel C-type lectin fold: implications for the NK cell-associated CD94/NKG2 receptors. Immunity 10, 75–82 (1999).
- Tormo, J., Natarajan, K., Margulies, D. H. & Mariuzza, R. A. Crystal structure of a lectin-like natural killer cell receptor bound to its MHC class Lligand. Nature 402, 623–631 (1999).
- Houchins, J. P., Yabe, T., McSherry, C. & Bach, F. H. DNA sequence analysis of NKG2, a family of related cDNA clones encoding type II integral membrane proteins on human natural killer cells. J. Exp. Med. 173, 1017–1020 (1991).
- Bauer, S. et al. Activation of NK cells and T cells by NKG2D, a receptor for stress-inducible MICA. Science 285, 727–729 (1999).
- Wu, J. et al. An activating immunoreceptor complex formed by NKG2D and DAP10. Science 285, 730–732 (1999).
- Wu, J., Cherwinski, H., Spies, T., Phillips, J. H. & Lanier, L. L. DAP10 and DAP12 form distinct, but functionally cooperative, receptor complexes in natural killer cells. J. Exp. Med. 192, 1059–1067 (2000).
- Bahram, S., Bresnahan, M., Geraghty, D. E. & Spies, T. A. A second lineage of mammalian major histocompatibility complex class I genes. Proc. Natl Acad. Sci. USA 91, 6259–6263 (1994).
- Bahram, S. & Spies, T.A. Nucleotide sequence of a human MHC class I MICB cDNA. Immunogenetics 43, 230–233 (1996).
- Groh, V. et al. Cell stress-regulated human major histocompatibility complex class I gene expressed in gastrointestinal epithelium. Proc. Natl Acad. Sci. USA 93, 12445–12450 (1996).
- Groh, V., Steinle, A., Bauer, S. & Spies, T. Recognition of Stress-Induced MHC Molecules by Intestinal Enithelial and T. Cells. Science 279, 1737-1740 (1998)
- Epithelial $\gamma\delta$ T Cells. Science **279**, 1737–1740 (1998). 23. Groh, V. et al. Broad tumor-associated expression and recognition by tumor-derived $\gamma\delta$ T cells of
- MICA and MICB. Proc. Natl Acad. Sci. USA 96, 6879–6884 (1999).
 Steinle, A., Groh, V. & Spies, T. Diversification, expression, and γ δ T cell recognition of evolutionarily distant members of the MIC family of major histocompatibility complex class I-related molecules. Proc. Natl Acad. Sci. USA 95, 12510–12515 (1998).
- Li, P. et al. Crystal Structure of the MHC Class I Homolog MIC-A, a γδT Cell Ligand. Immunity 10, 577–584 (1999).
- Weis, W. I., Kahn, R., Fourme, R., Drickamer, K. & Hendrickson, W.A. Structure of the calcium-dependent lectin domain from a rat mannose-binding protein determined by MAD phasing. Science 254, 1608–1615 (1991).
- Lawrence, M. & Colman, P. M. Shape complementarity at protein/protein interfaces. J. Mol. Biol. 234, 946–950 (1993)
- Sanchez, L. M., Chirino, A. J. & Bjorkman, P. J. Crystal structure of human ZAG, a fat-depleting factor related to MHC molecules. Science 283, 1914–1919 (1999).
- O'Callaghan, C.A. et al. Structural features impose tight peptide binding specificity in the nonclassical MHC molecule HLA-E. Mol. Cell 1, 531–541 (1998).
- Wilson, I.A. & Garcia, K. C. T-cell receptor structure and TCR complexes. Curr. Opin. Struct. Biol. 7, 839–848 (1997).
- Lo Conte, L., Chothia, C. & Janin, J. The atomic structure of protein-protein recognition sites. J. Mol. Biol. 285, 2177–2198 (1999).
- Vales-Gomez, M., Reyburn, H.T., Mandelboim, M. & Strominger, J. L. Kinetics of interaction of HLA-C ligands with natural killer cell inhibitory receptors. *Immunity* 9, 337–344 (1998).
- Chapman, T. L., Heikema, A. P. & Bjorkman, P.J. The Inhibitory Receptor LIR-1 Uses a Common Binding Interaction to Recognize Class I MHC Molecules and the Viral Homolog UL-18. *Immunity* 11, 463–432 (1909).
- Vales-Gomez, M., Reyburn, H.T., Erskine, R.A. & Strominger, J. Differential binding to HLA-C of p50-activating and p58-inhibitory natural killer cell receptors. Proc. Natl Acad. Sci. USA 95, 14326–14331 (1998).
- Vales-Gomez, M., Reyburn, H.T., Erskine, R.A., Lopez-Botet, M. & Strominger, J. L. Kinetics and peptide dependency of the binding of the inhibitory NK receptor CD94/NKG2-A and the activating receptor CD94/NKG2-C to HLA-E. EMBO J. 18, 4250–4260 (1999).
- Maenaka, K. et al. Killer cell immunoglobulin receptors and T cell receptors bind peptide-major histocompatibility complex class I with distinct thermodynamic and kinetic properties. J. Biol. Chem. 274, 28329–28334 (1999).
- 37. Davis, M. M. et al. Ligand recognition by $\alpha\beta$ T cell receptors. Annu. Rev. Immunol. 16, 523–544 (1998).
- Willcox, B. E. et al. TCR binding to peptide-MHC stabilizes a flexible recognition interface. Immunity 10, 357–365 (1999).
- 39. Gao, G. F. et al. Crystal structure of the complex between human CD8αα and HLA-A2. Nature 387, 630–634 (1997).
 40. Kern, P.S. et al. Structural basis of CD8 coreceptor function revealed by crystallographic analysis of a
- 40. Ref n, k 3. St dictural basis of CDs correceptor function revealed by crystallographic analysis of a murine CD8αα ectodomain fragment in complex with H-2Ks. Immunity, 5,19–530 (1998).
- de Vos, A. M., Ultsch, M. & Kossiakoff, A. A. Human growth hormone and extracellular domain of its receptor: crystal structure of the complex. Science 255, 306–312 (1992).
- Cerwenka, A. et al. Retinoic acid early inducible genes define a ligand family for the activating NKG2D receptor in mice. *Immunity* 12, 721–727 (2000).
 Wolan, D.W. et al. Crystal structure of the murine NK cell-activating receptor at 1.95 Å. *Nature*
- Immunol. 2, 248–254 (2001).

 44. Doublié. S. Preparation of Selenomethionyl Proteins for Phase Determination. *Meth. Enzymol.* 276.
- 523–531 (1997).

 45. Otwinowski, Z. & Minor, W. Processing of X-ray diffraction data collected in oscillation mode. *Meth.*
- Enzymol. 276, 307–327 (1997).
 46. Brünger, A. T. et al. Crystallography & NMR System: A New Software Suite for Macromolecular
- Structure Determination. Acta Cryst. D 54, 905–921 (1998).

 47. Jones, T.A. & Kjeldgaard, M. Electron density map interpretation. Meth. Enzymol. 277, 173–208 (1997).

 48. Berman, H. M. et al. The Protein Data Bank. Nucleic Acids Res. 28, 235–242 (2000).
- Bauer, S., Willie, S.T., Spies, T. & Strong, R. K. Expression, purification, crystallization and crystallographic characterization of the human MHC class I related protein MICA. Acta Cryst. D 54, 451–453 (1998).
- Ding, Y. H. et al. Two human T cell receptors bind in a similar diagonal mode to the HLA-A2/Tax peptide complex using different TCR amino acids. *Immunity* 8, 403–411 (1998)
- tide complex using different TCR amino acids. *Immunity* 8, 403–411 (1998).
 51. Nicholls, A., Sharp, K.A. & Honig, B. Protein folding and association: insights from the interfacial and thermodynamic properties of hydrocarbons. *Proteins Struct. Funct. Genet.* 11, 281–296 (1991).
- Brünger, A. T. Free R value: a novel statistical quantity for assessing the accuracy of crystal structures. Nature 355, 472–475 (1992).
- Laskowski, R. A., MacArthur, M. W., Hutchinson, E. G. & Thornton, J. M. PROCHECK: a program to check the stereochemical quality of protein structures. J. Appl. Cryst. 26, 283–291 (1992).